第 31卷第 12期　　焊　接　学　报　　Vol. 31　No. 12
2010年 12月　　TRANSACTIONS OF THE CHINA WELDING INSTITUTION　　December 2010

两级加载下两焊点拉剪点焊接头的损伤

王瑞杰[1]，　尚德广[2]，　刘泓滨[1]
（1. 昆明理工大学 机电工程学院，昆明　650093；
2. 北京工业大学 机械工程与应用电子技术学院，北京　100124）

王瑞杰

摘　要：对带有两个焊点的拉剪点焊试样进行了两级变幅疲劳加载，应力幅和平均应力均不相等．结果表明，两级变幅加载下存在应力次序效应．在低—高加载时存在“锻炼效应”，线性累积损伤的值大于 1；在高—低加载时存在“过载效应”，高—低加载下的线性累积损伤值也大于 1．在高—低加载方式下，高水平应力作用后，低水平应力剩余疲劳寿命大于按线性疲劳累积损伤法则所估算的剩余寿命，低应力作用下的剩余寿命甚至大于低应力单独作用下的全寿命．高—低加载下的线性累积损伤结果表明，焊点边缘更象是一个缺口．

关键词：点焊；两级加载；累积损伤；缺口效应
中图分类号：TG407　TH114　文献标识码：A　文章编号：0253－360X(2010)12－0077－04

0　序　　言

电阻点焊在现代机械制造工业中应用广泛，特别是在汽车、机车、地铁等车辆车身结构上，因而点焊在汽车生产中占有重要的地位[1]．点焊接头由焊核、热影响区和母材组成，它们具有不同的力学性能[2]．点焊联接发生疲劳破坏时，疲劳裂纹萌生于两板间焊点边缘处，垂直于板面向板外扩展，裂纹的萌生位置不便于观测；而且实际工作中的焊点常处于复杂应力状态，力学分析十分困难[3]，如何准确地预测焊点疲劳寿命始终是研究中的一个难点．

在对点焊疲劳行为的研究中，对焊点边缘有两种认识[4]，一种认为是已存在的裂纹，疲劳寿命即裂纹扩展寿命；另一种认为是一个缺口，疲劳寿命由裂纹萌生与扩展寿命组成．两者的区别在于是否存在裂纹萌生阶段．近来许多研究发现，全寿命中存在裂纹萌生阶段[5]，且占全寿命的比例相当大，焊点边缘不应视为裂纹．

工程构件常受复杂应力作用，因此复杂加载条件下材料的疲劳损伤问题受到广泛关注．特别是许多研究均以两级加载作为复杂加载的基本形式．汽车在行驶过程中，点焊接头受到的是复杂的应力．文中对两级应力作用下低碳钢点焊接头的损伤进行了研究，分析了焊点边缘的缺口效应．

1　两级加载试验分析

研究中采用的两焊点点焊试样的结构如图 1所示．图 1中，焊核直径 $d=5.4$ mm，两焊点位置对称，间距 30 mm，试样总长 $L=142$ mm，搭接长度 $l=62$ mm，试样宽度 $b=25.4$ mm，板厚 $\delta=1.5$ mm．材料为汽车车身用镀锌低碳钢板，弹性模量 $E=198.4$ GPa，泊松比 $\nu=0.29$，质量密度为 $\rho=7\,800$ kg/m³．文中疲劳试验均选用 MTS810－100 kN电液伺服材料试验机，应力波形选用三角波，加载频率为 5～15 Hz，施加应力方式均为应力控制，试验均在室温空气中进行．

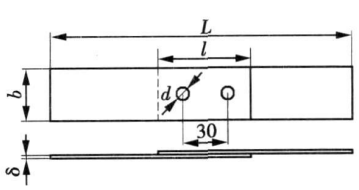

图 1　两焊点点焊试样的结构（mm）
Fig. 1　Specimen configuration of two-spot welds

试验中两级应力的组合方式为：低—高加载时，先在较低应力水平下作用到预定的循环比，然后在较高应力水平下加载，直到试样最终破坏，得到较高

收稿日期：2009－06－23
基金项目：昆明理工大学引进人才基金资助项目（2008ZC023M）

应力水平下的剩余寿命及剩余循环比; 高—低加载时, 先在较高应力水平下加载, 再在较低应力水平下加载.

在两级加载试验中, 根据已有的恒幅载荷作用下的疲劳试验数据, 选择两个应力水平. 在一个应力水平下作用一定应力循环数后, 再在另一个应力水平下加载直到试样失效, 分别得到两个应力水平下的应力循环数. 如文献 [6]所述, 在恒幅载荷作用下, 得到的名义应力幅—寿命关系如图 2所示. 为能够查明两个应力水平下加载次序对疲劳性能的影响, 确定这两个应力水平时, 要求对应的疲劳寿命应有较明显的差别. 根据已有的疲劳试验结果, 所选取的两级应力应力水平如表 1所示. 此时应力水平一下的疲劳寿命 N_1 约为应力水平二下的疲劳寿命 N_2 的 3倍.

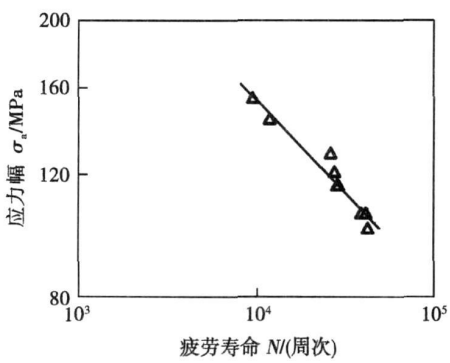

图 2 恒幅载荷下的应力幅与寿命关系全对数坐标

Fig. 2 Relation of stress amplitude and life under constant amplitude loading

表 1 两级加载的应力水平与疲劳寿命

Table 1 Stress levels and fatigue lives for two-level loading

应力水平	平均应力 σ_m/MPa	应力幅 σ_a/MPa	疲劳寿命 N(周次)
水平一	120.51	115.38	28 548
水平二	158.97	153.85	9 694

在表 1所示的不同加载应力水平下, 对试样施加循环应力, 循环数达到第一个应力水平下的循环数 n_1 后暂停试验, 改变应力水平, 再在应力水平二下施加循环应力直到试样最终疲劳破坏, 记录试样在第二级应力下的疲劳寿命即试验剩余寿命 n_2. 低—高加载和高—低加载下的疲劳寿命试验结果分别如表 2, 表 3所示.

将使用 Miner线性疲劳累积损伤法则估算的第二级应力作用下的剩余寿命 n_{2r} 也分别表示在相应的表格中. 表中 n_1/N_1 为第一个应力水平作用到的循环比.

表 2 低—高应力循环加载

Table 2 Fatigue lives under low-high loading

编号	应力水平一的循环数 n_1(周次)	应力水平一的循环比 n_1/N_1	预计剩余寿命 n_{2r}(周次)	试验剩余寿命 n_2(周次)
D37	4 000	0.14	8 337	7 321
D36	8 000	0.28	6 980	7 174
D35	18 000	0.63	3 587	3 811
D45	18 000	0.63	3 587	3 105
D34	24 000	0.84	1 551	5 531

表 3 高—低应力循环加载

Table 3 Fatigue lives under high-low loading

编号	应力水平一的循环数 n_1(周次)	应力水平一的循环比 n_1/N_1	预计剩余寿命 n_{2r}(周次)	试验剩余寿命 n_2(周次)
D33	1 000	0.10	25 693	43 952
D32	2 000	0.21	22 553	50 171
D46	2 000	0.21	22 553	49 025
D31	4 000	0.41	16 843	37 723
D30	6 000	0.62	10 848	17 863

2 两级加载下的线性累积损伤结果

表 2与表 3中的第二级应力作用下的疲劳寿命数据表明, 对于低—高加载, 第二级应力作用下的剩余寿命 n_2 均小于试样在第二级应力水平单独作用下的全疲劳寿命 N_2, 这与线性疲劳累积损伤理论较为一致. 而对于高—低加载情况, 在第二级应力作用下的剩余寿命 n_2 结果中出现了大于其在第二级应力水平单独作用下的全疲劳寿命 N_2 的情况, 且有多个试样有这样的寿命结果, 出现这种情况的原因有待于进一步分析.

使用 Miner线性疲劳累积损伤法则, 对于表 2所示的低—高加载与表 3所示的高—低加载下的试验数据, 分别计算前后两次加载的循环比, 得到两级应力作用下的累积疲劳损伤. 低—高、高—低加载的累积损伤值 $\Sigma n_i/N_i$ 分别如表 4, 表 5所示. n_2/N_2 为第二级应力水平下的循环数占第二级应力水平下疲劳寿命的循环比. N_i 为第 i个应力水平下的疲劳寿命.

对于表 4与表 5中低—高与高—低加载的两组试样, 将线性累积损伤结果随第一级应力循环比 n_1/N_1 增加的变化分别表示在图 3与图 4中. 由图 3与图 4可见, 累积损伤数据均有这样的规律: 随着较小应力水平下的循环数增加, 疲劳损伤累积值增加;

而随着较大应力水平下循环数的增加，疲劳损伤累积值有减少的趋势．显然，这与疲劳损伤累积理论相一致，即疲劳寿命取决于加载的次序．

表 4　低—高加载下的线性累积损伤

Table 4　Linearly cumulated damage under low-high loading

编号	应力水平一的循环数 n_1(周次)	应力水平一的循环比 n_1/N_1	应力水平二的循环比 n_2/N_2	累积损伤 $\sum n_i/N_i$
D37	4 000	0.14	0.76	0.90
D36	8 000	0.28	0.74	1.02
D35	18 000	0.63	0.39	1.02
D45	18 000	0.63	0.32	0.95
D34	24 000	0.84	0.57	1.41

表 5　高—低加载下的线性累积损伤

Table 5　Linearly cumulated damage under high-low loading

编号	应力水平一的循环数 n_1(周次)	应力水平一的循环比 n_1/N_1	应力水平二的循环比 n_2/N_2	累积损伤 $\sum n_i/N_i$
D33	1 000	0.10	1.54	1.64
D32	2 000	0.21	1.76	1.97
D46	2 000	0.21	1.72	1.92
D31	4 000	0.41	1.32	1.73
D30	6 000	0.62	0.63	1.25

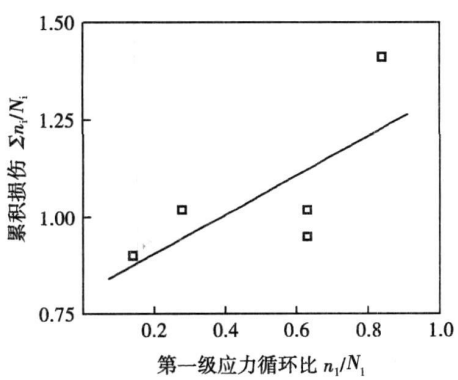

图 3　低—高加载下线性累积损伤与第一级应力循环比

Fig. 3　Linearly cumulated damage and the first stress level life ratio under low-high loading

对于低—高加载，由疲劳累积损伤理论可知，受由低到高的加载次序的影响，使用 Miner线性损伤累积法则得到的累积损伤值呈现大于 1的趋势，图 3的累积损伤值与此趋势基本符合．随着低应力水平加载循环数的增多，累积损伤值的趋势为从小到大，即随着在较低应力下的循环数的增多，总疲劳寿命变长，出现了明显的“锻炼效应”．由此可见，对于点焊试样，在低—高加载的情况下，加载次序对累积损伤有明显的影响．

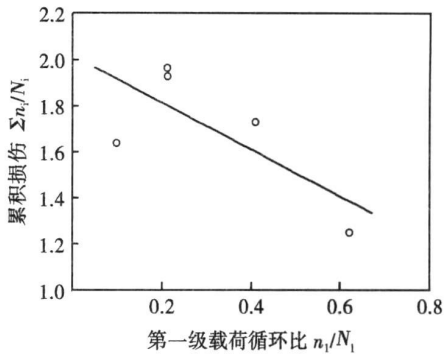

图 4　高—低加载下线性累积损伤与第一级应力循环比

Fig. 4　Linearly cumulated damage and the first stress level life ratio under high-low loading

对于高—低加载，由图 4的累积损伤值可见，受由高到低的加载次序的影响，随着较大应力水平循环数的增加，线性疲劳损伤累积值有减小的趋势．由此可见点焊试样在高—低加载情况下，应力次序对疲劳累积损伤也有明显地影响．在高—低加载方式下，由于试样的剩余试验寿命均出现了大于由线性累积损伤法则所估计的剩余寿命的情况，因而此处的累积损伤值均大于 1.

由以上分析可以得出结论，在非等平均应力非等应力幅的两级应力作用下，加载次序对于两点拉剪点焊试样的疲劳累积损伤有明显的影响．

3　结果讨论

在试验中，所施加的两级应力水平的特点是，应力幅不同，平均应力也不相同．由 Forman疲劳裂纹扩展公式可知，平均应力对于裂纹扩展速率有明显的影响，当平均应力降低时，裂纹扩展速率大为降低．另外，高低幅度的应力交替作用时，高应力峰(或过载峰)的出现，对随后的低应力等幅循环的裂纹扩展速率的影响，与对疲劳损伤的影响有相同的趋势．即过载峰的存在对于随后的低应力循环的裂纹扩展速率有明显的延缓作用[7].

一般情况下，由累积损伤理论可知，若按低—高加载次序，则无论是光滑件还是缺口件，疲劳破坏时线性累积损伤值 $\Sigma n_i/N_i$一般均大于 1. 但若按高—低加载次序，钢制缺口件有两种情况，即合金钢累积损伤值小于 1，而低碳钢累积损伤平均值大于 1；钢制光滑件累积损伤 $\Sigma n_i/N_i$一般常小于 1[8].

在文中研究的高—低加载下，在高的平均应力和大的应力幅作用一段时间后，剩余的疲劳寿命均明显大于按线性疲劳累积损伤理论所计算的剩余损

伤所对应的低水平应力下的剩余寿命值，甚至出现了大于低应力单独作用下全疲劳寿命的情况．这样，所得到的剩余损伤值较大，甚至出现了剩余损伤值大于 1的情况，从而导致用线性损伤法则累积的损伤值大于 1．这与低碳钢材料试样缺口件在高—低加载时的结论类似，因而这也是将焊核边缘视为一个缺口的一个佐证．在焊点处两板接触面类似于一个环形缺口，在缺口附近有严重的应力集中，而焊点边缘区域材料性能变化很大，一定位置处利于裂纹萌生．

4 结 论

（1）点焊试样在低—高两级加载情况下，线性累积损伤存在“锻炼效应”．

（2）点焊试样在高—低应力作用下，存在“过载效应”，线性累积损伤值大于 1．

（3）点焊试样的焊点边缘在疲劳破坏过程中应视为是一个缺口．

参考文献：

[1] Zhou Mingxing. A unified approach to accessing the mechanical performance of resistance spot welds[D]. Ann Arbor: University of Michigan, 2001.

[2] 常保华，史耀武，董仕节．点焊搭接接头中的应力分布及接头疲劳行为研究[J]．机械强度，1998，20(4)：271—277.
Chang Baohua, Shi Yaowu, Dong Shijie. Studies on stress distribution in spot welded lap joints and the fatigue behavior of the joints[J]. Journal of Mechanical Strength, 1998, 20(4): 271—277.

[3] 薛 河．点焊结构应力应变场数值模拟分析[J]．汽车技术，2002(10)：33—35.
Xue He. Numerical simulating analysis of stress and strain field of spot welding structure[J]. Automobile Technology, 2002(10): 33—35.

[4] Sheppard S D, Pan N. A look at fatigue in resistance spot welds—notch or crack[C]// SAE2001 World Congress Technical Paper. Society of Automotive Engineers, Detroit, USA, 2001: 462—475.

[5] Sheppard S D, Strange M. Fatigue life estimation in resistant spot welds: Initiation and Early Growth Phase[J]. Fatigue and Fracture of Engineering Materials and Structures, 1992, 15(6): 531—549.

[6] 王瑞杰，尚德广，李力森，等．两点拉剪点焊试样疲劳过程中的固有频率[J]．实验室研究与探索，2007，26(11)：207—210.
Wang Ruijie, Shang Deguang, Li Lisen, et al. Frequency change of tension shear two spot welds during fatigue[J]. Research and Exploration in Laboratory, 2007, 26(11): 207—210.

[7] 陈传尧．疲劳与断裂[M]．武汉：华中科技大学出版社，2002.

[8] 郑修麟．金属疲劳的定量理论[M]．西安：西北工业大学出版社，1994

作者简介：王瑞杰，男，1972年出生，博士，副教授，硕士研究生导师．主要从事机械结构强度及现代机械设计理论与方法、高速高效切削加工方面的科研和教学工作．发表论文 20余篇．

Email: wrj@kmust.edu.cn

Microstructures and properties of SiC_w/2024Al MMCs joint by capacitor discharge welding XU Feng, ZHAI Qiuya, XU Jinfeng (1. School of Material Science and Engineering, Shaanxi University of Technology, Hanzhong 723003, China; 2. School of Material Science and Engineering, Xi'an University of Technology, Xi'an 710048, China). p. 57—60

Abstract: The capacitor discharge spot welding on SiC_w/2024Al alloy matrix composite sheet with 0.2 mm thickness was study. The microstructures and properties of the joint were analyzed, and the temperature field and cooling rate of nugget were calculated. The results show that the joint microstructure consists of nugget zone, heat-affected zone and semi-melt zone. The cooling rate of the joint reaches to 5.25×10^6 K/s. The microstructure of the nugget is obviously refined and the SiC-Al interfacial reaction is not found in the middle of the joint because of high cooling rate. The width of semi-melt zone is 10 to 15 μm, which divides the nugget zone and base metal. The microstructure of heat-affected zone is not obviously coarse and keeps conformation with base metal. To obtain the high quality spot weld joint, the welding parameters are a welding voltage of 80 V, a capacitor of 3 300 μF and a electrode pressure of 18 N.

Key words: composite material; SiC whisker reinforced Al alloy matrix composites; capacitor discharge welding; microstructures and properties of joint

Robust joint tracking with structured-light vision sensing GONG Yefei, DAI Xianzhong, LI Xinde, ZHANG Jie (Key Laboratory of Measurement and Control of Complex Systems of Engineering, Ministry of Education, Southeast University, Nanjing 210096, China). p. 61—64

Abstract: The performance of joint feature extraction is degraded greatly during welding because of severe disturbances, so a prediction-matching-estimation combined close-looped iterated method is proposed for weld feature tracking. The position and shape of the joint stripe profile in the image is predicted at first, then the joint is recognized by a model-based profile matching method, and lastly the weld trajectory is filtered and estimated based on the confidence of the extracted feature. Experiments show that the method promotes the joint recognition results to ensure a robust and real-time weld seam tracking even in the face of gross error or failure occurrence in joint feature extraction.

Key words: joint tracking; structured-light vision; prediction; filtering

High-temperature oxidation behavior of cerium on the surface of Sn-Zn lead-free solders WANG Hui, LIU Xincai, PAN Jing, MA Yongcun (Faculty of Materials Science and Chemical Engineering, Ningbo University, Ningbo 315211, China). p. 65—69

Abstract: The distribution and existing form of Ce on the surface of Sn-9Zn-0.15Ce and Sn-9Zn-0.002Al-0.2Ga-0.25Ag-0.15Ce solder are investigated by atomic emission spectrometry and X-ray photoelectron spectroscopy. Results indicate that Ce enriches on the surface of the Sn-9Zn-0.15Ce solder in the range of 0 to 40 nm. The concentration of Ce in the enriched zone is about 30 at%, which is 250 times of that in the bulk solder, and the enriched Ce on the surface is mostly oxidized as CeO_2 and Ce_2O_3. With the multi-addition of Ga and Al in the Sn-9Zn-0.002Al-0.2Ga-0.25Ag-0.15Ce solder, Ga enriches in range of 0 to 6 nm on the surface, while Al enriches in range of 2 to 20 nm in oxidized form. The Ce-enriched layer is in the range of 2 to 60 nm on the surface covered by the Ga and Al enriched layers, and the oxidation of Ce is depressed significantly.

Key words: Sn-Zn; lead-free solder; Ce; oxidation; surface enrichment

Influence of ceria on phosphorus and sulphur of low alloy steel weld FAN Xiying, GUO Yonghuan (College of Mechanical and Electrical Engineering, Xuzhou Normal University, Xuzhou 221116, China). p. 70—72

Abstract: The coating of E5515-G, a low alloy steel electrode, was added in different amount of ceria (CeO_2) for enhancing electrode properties which was studied by means of impact toughness, metallographic examination and X-ray fluorescence spectrometry test. The results show that the proper addiction of CeO_2 is beneficial to the desulfurization and dephosphorization of the weld and improves the impact absorbed energy of deposited metal. Different addition amount of CeO_2 can lead to various desulfurization efficiency, which makes a great difference, whereas the dephosphorization efficiency is unconspicuous. The microstructures of the weld can be effectively made fine by adding CeO_2 into electrode coating, but the addition amount of CeO_2 should be proper. The microstructure of the weld is the finest when the addition amount of CeO_2 is 3%. When the amount of CeO_2 is optimal, the S content in weld metal will decrease by 58.128 1%, while the P content 14.285 7%.

Key words: ceria; low alloy steel electrode; weld; sulphur; phosphorus

Numerical simulation on keyhole thermal effect of vacuum electron beam welding of magnesium alloy LUO Yi[1,2], LIU Jinhe[1], YE Hong (1. School of Material Science and Engineering, Northwestern Polytechnical University, Xi'an 710072, China; 2. School of Material Science and Engineering, Chongqing Institute of Technology, Chongqing 400050, China). p. 73—76

Abstract: The keyhole thermal effect of vacuum electron beam welding for magnesium alloy was analyzed. In view of the thermal effect of high-temperature metal vapor and the deep-penetration effect of keyhole during welding, a composite heat source model applying to magnesium alloy, which was made up of Gaussian surface source and cone body source, was developped. By the different valuation to the power coefficients of Gaussian surface source and cone body source, the various focus states of electron beam were simulated to get the welding temperature fields. And then, the simulation results were favorable for the shape calculation to keyholes and welds. The experimental results show that the simulation results have good consistency with the experiment welds.

Key words: magnesium alloy; vacuum electron beam welding; composite heat source model; keyhole; thermal effect; weld shape

Damage of two-spot welds under two level loading WANG Ruijie, SHANG Deguang, LIU Hongbin[1] (1. Faculty

of Mechanical and Electrical Engineering, Kunming University of Science and Technology, Kunming 650093, China; 2. College of Mechanical Engineering and Applied Electronics, Beijing University of Technology, Beijing 100124, China). p. 77—80

Abstract: Two-level loadings of unequal stress amplitude and unequal mean stress were applied on the two-spot tension-shear spot welds. Experimental results show that there exists stress sequence effect under two-level loading. There exists exercise effect under low-high loading: the damage accumulated by linear damage accumulation rule is higher than 1; there exists overload retardation under high-low loading: the damage accumulated by linear damage accumulation rule is also over 1. Under high-low loading, residual lives under low stress level are longer than residual life calculated from linear damage accumulation rule; some residual fatigue lives are even longer than total life under low stress alone. The damage accumulation result under high-low loading indicates that the periphery of spot welds behaves as a notch.

Key words: spot weld; two-level loading; damage accumulation; notch effect

Effects of forming process of combustion welding rod on manual SHS welding

LI Zhizun, XIN Wentong, HU Renxi, HAN Fengqi (Department of Basic Course, Ordnance Engineering College, Shijiazhuang 050003, China). p. 81—84

Abstract: The influence of forming process of the combustion rod on manual self-propagating high-temperature synthesis (SHS) welding was investigated systematically, and the optimum parameters were obtained. Results showed that the particle size, the forming density and the mixing time had significant effects on the combustion reaction and the welding quality. As the particle size of the powder increased, welding spatter became severe and a lot of stomata generated in the seam. As the particle size decreased, the combustion velocity increased and the rod was difficult to operate. The optimum particle size to make combustion rod was −260 to +300 mesh. It was showed that there was a peak in the forming density and combustion velocity curve. The optimum forming density was between 2.74 and 3.05 g/cm³. Results also showed that when the mixing time increased, the reaction and spatter became violent. But if the mixing time was too short, the powder could not contact adequately and the heat generated was not enough to melt the metal. The optimum mixing time was 30 min. It was showed that the diameter of the rod had not obvious effect on the combustion, and it could be determined by the thickness of the weldment.

Key words: manual self-propagating high-temperature synthesis welding; combustion welding rod; forming technology

Effect of process parameters on strengthening of steel surface with Fe-Al intermetallic compounds

ZHANG Deku, WANG Kehong, ZHANG Jing, ZHAO Nan (School of Materials Science and Engineering, Nanjing University of Science and Technology, Nanjing 210094, China). p. 85—88

Abstract: The intermetallic compound Fe_3Al was prepared by plasma arc surface remelting, in which the mixture of Al powder and Fe powder was coated on the surface of Q235 steel. The effect of plasma arc surfacing parameters on form of coating was studied, and appropriate process parameters were obtained. The microstructures and the measured Vickers hardness of the coating were analyzed. The results indicate that the variation of process parameters such as current, swing frequency of welding torch and travel speed closely relates with heat input, which has influence on microstructure, melting state of substrate, interface bonding of substrate and coating, and thus the corrosion and wear resistance of the coating is improved greatly. The optimum surfacing parameters are a current of 130 A, a travel speed of 5 cm/min, a swing amplitude of 4 mm and a frequency of 0.4 Hz under this experiment condition.

Key words: plasma arc surfacing; intermetallic compounds; microhardness

Metallograph and high-temperature impact toughness of circumferential joint by SAW of BHW35 steel

WANG Xianyun[1,2], WANG Wenxian[2], HAO Ruihua[1] (1. Taiyuan Boiler Group Co., Ltd., Taiyuan 030021, China; 2. College of Materials Science and Engineering, Taiyuan University of Technology, Taiyuan 030024, China). p. 89—92, 96

Abstract: BHW35 steel was welded by automatic submerged-arc welding (SAW) with H08Mn2MoA welding wires and flux HJ350. After stress relief annealing by the postweld heat-treatment system, impact tests on welded joint and base metal were carried out at 20, 100, 200 and 350 ℃, and the scanning electron microscopy (SEM) fractograph, metallograph, hardness and chemical compositions of welding seam were analyzed. The results indicate that the highest hardness of HAZ is 291.6 HV. The toughness increases greatly compared with that at room temperature. The temperature peak value of impact absorbing energy of welding seam occurs at weld of 100 ℃ and both HAZ and base metal of 200 ℃. The impact toughness in HAZ is better than that in welding seam. The impact absorbing energy of welded joint is over 47.33 J at room temperature and 134.67 J at 350 ℃, which meets the toughness demand for the welded joint and base metal. SEM fractograph indicates that all impact fractures of base metal exhibit ductile dimple, and the impact fractures in welded joint at room temperature exhibit quasi-cleavage and ductile dimple. With the temperature increasing, the fractures subjected high temperature impact all exhibit ductile dimple, the better toughness is, the more obvious tearing feature of ductile dimple is, and the larger the ductile dimple is, the more obvious non-uniform distribution is.

Key words: BHW35 steel; submerged-arc weld joint; metallograph and hardness; impact absorbing energy; fractograph

Welded joint properties of X60 pipeline steel at −20 ℃

LI Jianjun[1,2], DU Zeyu[1], LIU Guangyun[2], LÜ Xiangyang[2] (1. Material School, Tianjin University, Tianjin 300072, China; 2. China Petroleum Pipeline Welding Training Center, Langfang 065000, China). p. 93—96

Abstract: In accordance with the site construction of X60 pipeline steel at −20 ℃, the mechanical properties, metallographic structure, hardness, Charpy impact absorbing energy and the fracture structure of the girth welded joints of φ711 × 15.9 mm pipeline are analyzed. The results show that the highest HAZ hardness value of the X60 pipe steel joints girth-welding